How photosynthetic reaction centers control oxidation power in chlorophyll pairs P680, P700, and P870

Hiroshi Ishikita[†], Wolfram Saenger, Jacek Biesiadka, Bernhard Loll[‡], and Ernst-Walter Knapp[§]

Institute of Chemistry and Biochemistry, Free University Berlin, Takustrasse 6, D-14195 Berlin, Germany

Edited by Harry B. Gray, California Institute of Technology, Pasadena, CA, and approved May 11, 2006 (received for review February 21, 2006)

At the heart of photosynthetic reaction centers (RCs) are pairs of chlorophyll *a* (Chl*a*), P700 in photosystem I (PSI) and P680 in photosystem II (PSII) of cyanobacteria, algae, or plants, and a pair of bacteriochlorophyll *a* (BChl*a*), P870 in purple bacterial RCs (PbRCs). These pairs differ greatly in their redox potentials for one-electron oxidation, E_m. For P680, E_m is 1,100–1,200 mV, but for P700 and P870, E_m is only 500 mV. Calculations with the linearized Poisson–Boltzmann equation reproduce these measured E_m differences successfully. Analyzing the origin for these differences, we found as major factors in PSII the unique Mn_4Ca cluster (relative to PSI and PbRC), the position of P680 close to the luminal edge of transmembrane α-helix d (relative to PSI), local variations in the cd loop (relative to PbRC), and the intrinsically higher E_m of Chl*a* compared with BChl*a* (relative to PbRC).

electron transfer | photosystem | redox potential | special pair | electrostatic energy

The essence of photosynthetic reaction centers (RCs) of photosystem I (PSI) and photosystem II (PSII) of cyanobacteria, green algae, and plants, as well as of purple bacterial RCs (PbRCs), are two homologous protein subunits (D1, D2) in PSII, (L, M) in PbRC, and the C-terminal RC domains of subunits (A, B) in PSI. The polypeptide chains of these subunits and the C-terminal domains of PSI are folded into five transmembrane α-helices (TMHs) in a semicircular arrangement, and the two subunits in each RC are interlocked in a handshake motif with comparable topography and related by a pseudo-twofold symmetry axis (Fig. 1).

We consider here the pair of chlorophyll *a* (Chl*a*) in PSI (Chl*a* $P_{A/B}$ in P700) and in PSII (Chl*a* $P_{D1/D2}$ in P680) and the pair of bacteriochlorophyll *a* (BChl*a*) in PbRC (BChl*a* $P_{L/M}$ in P870), where light-driven charge separation results in positively charged radicals $P700^{+\cdot}$, $P680^{+\cdot}$, and $P870^{+\cdot}$, respectively. In PSI and PbRC, $P700^{+\cdot}$ and $P870^{+\cdot}$ are rereduced by small water-soluble proteins. By contrast, $P680^{+\cdot}$ in PSII is rereduced by a redox-active tyrosine (D1-Tyr-161, Y_Z), which is subsequently reduced by electron transfer from the unique Mn_4Ca cluster, where water is oxidized under release of atmospheric oxygen, protons, and electrons. Kinetic studies (1) and computations (2) yielded redox potentials for one-electron oxidation E_m(P680) of 1,100–1,300 mV, high enough for $P680^{+\cdot}$ to act as an electron acceptor for the different Mn_4Ca redox states. According to recent studies, P680 probably consists of the Chl*a* pair $P_{D1/D2}$ or the two adjacent accessory Chl*a*, $Chl_{D1/D2}$ (3).

In contrast to PSII, with an unusually high E_m(P680) of 1,100–1,300 mV (1, 2), the corresponding E_m values in PbRC, E_m(P870) = 500 mV (4), and in PSI, E_m(P700) = 500 mV (5), are low. Part of these E_m differences were associated with electronic coupling, which is weak between Chl*a* in $P_{D1/D2}$ but strong between Bchl*a* in $P_{L/M}$ because of mutual overlap of BChl*a* rings I. Indeed, in the PbRC mutant His(M202)Leu, where His-202 that coordinates BChl*a* P_M is lost, P_M is replaced by bacteriopheophytin *a*, yielding a larger measured value of $E_m(P_L)$ = 640 mV (6). A significant part of this E_m difference (140 mV) may be due to absence of strong electronic coupling. In this regard, it is noteworthy that P700 in PSI features an E_m of ≈500 mV (5), similar to E_m(P870), whereas mutual overlap of Chl*a* rings in P700 is absent in contrast to P870. Therefore, electronic coupling cannot explain the dramatic E_m difference of 600 mV between P680 and P870/P700. Although BChl*a* and Chl*a* dissolved in CH_2Cl_2 exhibit E_m(BChl*a*) = 640 mV (7) and E_m(Chl*a*) = 800 mV (8, 9), respectively (see supporting information, which is published on the PNAS web site), there remains a gap of 440 mV between E_m(P870) and E_m(P680) that has to be explained.

Although nature uses the same type of cofactors (Chl*a*) for $P_{A/B}$ in PSI and $P_{D1/D2}$ in PSII, the protein environment modulates their E_m such that E_m(P700) ≈ 500 mV in PSI is ≈700 mV lower than E_m(P680) = 1,200 mV in PSII. This redox potential difference is because in PSII, the oxidative power must be high enough to oxidize water with an E_m of 820 mV, whereas in PSI and PbRC, high oxidative power is not needed but the reducing power of released electrons is maximized, and, simultaneously, oxidative damage of the protein environment due to positively charged dimer radicals is prevented, evident by the fact that E_m is low for $P_{A/B}$ and $P_{L/M}$. To elucidate this known but still unexplained difference in E_m(P700), E_m(P870), and E_m(P680), we calculated E_m in the RC of PSI, PbRC, and PSII by solving the linearized Poisson–Boltzmann equation for all atoms in the crystal structures (10–14) under identical computational conditions. Former theoretical work mainly contributed to unravel the energetics of the primary electron transfer events in PbRC [i.e., the relative energy of the P*B and P^+B^- states (15–18)]. The aim of the present study was to understand how nature invokes the dramatic differences in BChl*a* and Chl*a* redox potentials solely by the surrounding protein matrix in PbRC, PSI, and PSII.

Results and Discussion

$E_m(P_{L/M})$ in PbRC. In WT PbRC, E_m(P870) was measured to be 500 mV (4). We calculated averages of $E_m(P_L)$ and $E_m(P_M)$ for different crystal structures (10, 11) of WT PbRC from *Rhodobacter sphaeroides* and obtained $E_m(P_L)$ = 635 ± 12 mV and $E_m(P_M)$ = 660 ± 14 mV (Fig. 2). The experimentally observed larger spin density on P_L [spin-density ratio $\rho(P_L)/\rho(P_M)$ = 0.72/0.28 (19)] can be attributed to larger localization of the cationic state at P_L, rendering $E_m(P_L) < E_m(P_M)$. Al-

Conflict of interest statement: No conflicts declared.

This paper was submitted directly (Track II) to the PNAS office.

Abbreviations: RC, reaction center; PbRC, purple bacterial RC; PSI, photosystem I; PSII, photosystem II; TMH, transmembrane α-helix; Chl*a*, chlorophyll *a*; BChl*a*, bacteriochlorophyll *a*.

[†]Present address: Department of Chemistry, Pennsylvania State University, 104 Chemistry Building, University Park, PA 16802.

[‡]Present address: Abteilung für Biomolekulare Mechanismen, Max-Planck-Institut für Medizinische Forschung, 69126 Heidelberg, Germany.

[§]To whom correspondence should be addressed. E-mail: knapp@chemie.fu-berlin.de.

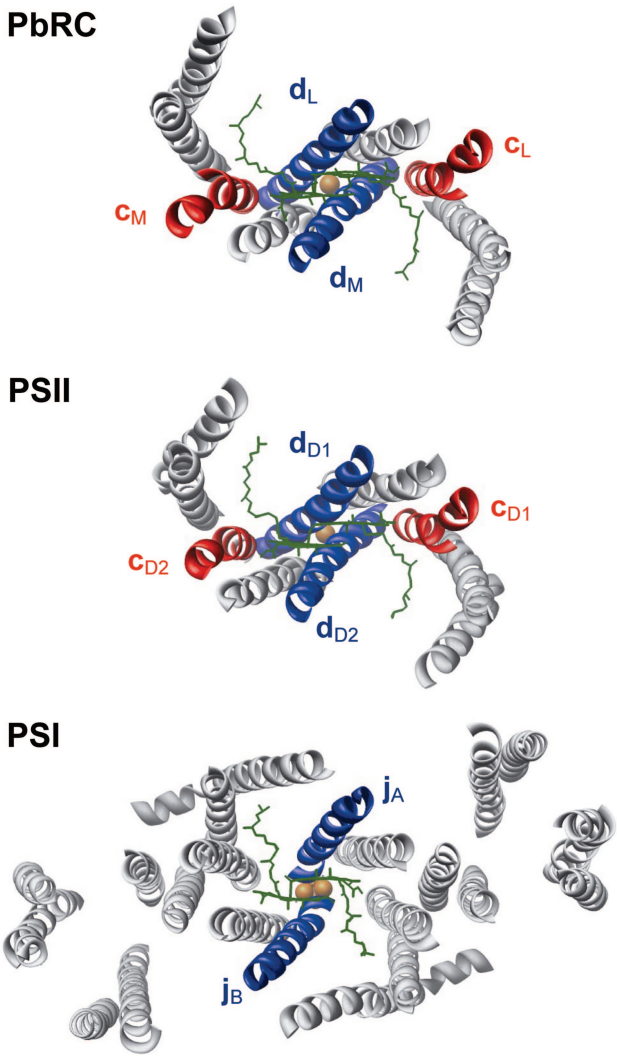

Fig. 1. Helices in RCs of PbRC, PSII, and PSI (view from the luminal side). Chlorophyll pairs are shown in green. RC subunits L, D1, A, M, D2, and B are shown in light gray. Helices **d** in PbRC/PSII and **j** in PSI (blue) provide axial ligands to $P_{L/M}/P_{D1/D2}$ and $P_{A/B}$, respectively, which are indicated in black. Helices **c** (red) are shown in PbRC/PSII. The non-heme Fe in PbRC/PSII and the Fe_4S_4 cluster F_X in PSI (orange) indicate the pseudo-C_2 symmetry axis that is normal to the paper plane.

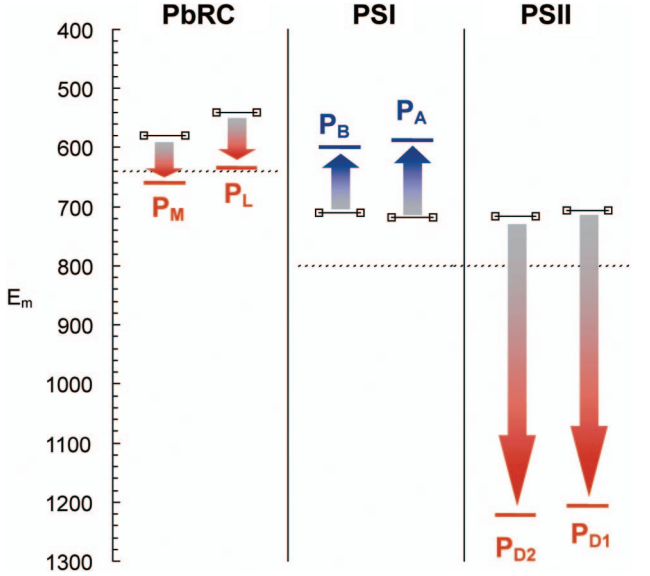

Fig. 2. Calculated E_m(BChl*a*) in PbRC and E_m(Chl*a*) in PSII (red horizontal bars) and PSI (blue horizontal bars). Dotted lines indicate the reference values measured for BChl*a* and Chl*a* dissolved in CH_2Cl_2: E_m(BChl*a*) = 640 mV (7) and E_m(Chl*a*) = 800 mV (8, 9). Horizontal bars with open squares at both ends refer to E_m(BChl*a*) and E_m(Chl*a*) calculated in protein dielectric volumes in the absence of atomic charges. The E_m shift from uncharged protein dielectric volume to charged protein environment is indicated by the vertical arrows.

though the calculated $E_m(P_L)$ is slightly lower than $E_m(P_M)$, the calculated E_m difference is in the same range of error as derived from three different PbRC crystal structures. To explain the measured spin-density distribution on P_L and P_M, electronic and vibronic coupling must also be considered (20, 21). The present study provides E_m only for monomer $P_{L/M}$, without considering these influences.

Because of large overlap of the BChl*a* rings I in P_L and P_M, it was suggested that the π–π interactions of the BChl*a* are strong in P870 of bacterial RC, whereas there is negligible overlap for the Chl*a* in P700 of PSI (13). The corresponding pair in PbRC mutant His(M202)Leu (12) consists of BChl*a*/bacteriopheophytin *a* (Bpheo*a*) at $P_{L/M}$ positions and is assumed to be a suitable model system that lacks electronic coupling between P_L and P_M. To estimate the electronic coupling effect on E_m(P870), we calculated $E_m(P_L)$ = 639 mV in the PbRC mutant His(M202)Leu (12), in excellent agreement with the measured value of 640 mV (6). In the present study, we calculated the E_m for both monomer BChl*a* in $P_{L/M}$, without considering possible couplings between them (20, 21). Under these computational conditions, the electrostatic influence on BChl*a* (P_L) generated by BPheo*a* (P_M) in mutant PbRC should be similar as that generated by BChl*a* (P_M) in WT PbRC, because both BChl*a* and BPheo*a* have the same net charge of zero in their uncharged states. Replacement of P_M ligand His at M202 by Leu deceases locally the polarity but not the charge. Hence, the effect on $E_m(P_L)$ should be small. Thus, as suggested previously (6), $E_m(P_L)$ in the PbRC mutant His(M202)Leu seems to refer to $E_m(P_L)$ of the WT PbRC, ignoring possible coupling between P_L and P_M.

***E_m* of RC Chlorophylls in PSI and PSII.** Our computations for PSI yielded $E_m(P_{A/B})$ = 587/599 mV (Fig. 2), ≈100 mV higher than the measured E_m(P700) = 500 mV (reviewed in ref. 5) that we ascribe to neglect of electronic coupling. In PSI, the calculated $E_m(A_{-1\,A/B})$ for the accessory Chl*a* are 833/815 mV (supporting information), ≈220–250 mV higher than those calculated for $P_{A/B}$.

In contrast, in PSII, the calculated $E_m(P_{D1})$ = 1,206 mV and $E_m(P_{D2})$ = 1,222 mV for the Chl*a* pair are slightly lower than the respective values $E_m(Chl_{D1})$ = 1,262 mV and $E_m(Chl_{D2})$ = 1,320 mV for the accessory Chl*a* (Fig. 4), indicating that the charge-separated state in PSII is stabilized with positive charge localized at $P_{D1/D2}$ rather than at the accessory $Chl_{D1/D2}$ showing >40 mV higher E_m (22).

Main Contributions to the 600-mV E_m Difference Between $P_{D1/D2}$ in PSII and $P_{A/B}$ in PSI. ***Peripheral protein subunits up-shifting $E_m(P_{D1/D2})$ by 200 mV.*** Upon removal of all protein subunits except for the D1/D2 subunits of PSII harboring the RC, the calculated $E_m(P_{D1/D2})$ is down-shifted to 1,032/1,019 mV (Fig. 4), indicating that 170–200 mV of the 600-mV difference between $E_m(P_{D1/D2})$ and $E_m(P_{A/B})$ originates from the atomic charges and protein dielectric volume of all PSII subunits except for D1/D2. The protein volume is defined as the volume obtained by merging the volumes of the van der Waals spheres of all protein atoms by using CHARMM atomic radii. In protein dielectric volume, a homogeneous

Table 1. Direct influence of cofactor/protein charges on E_m(BChl*a*) in PbRC (L/M) and E_m(Chl*a*) in PSI RC (PsaA/PsaB) and PSII RC (D1/D2)

Components of protein	PbRC				PsaA/PsaB				D1/D2			
	M		L		B		A		D2		D1	
	B_M	P_M	P_L	B_L	A_{-1B}	P_B	P_A	A_{-1A}	$Ch1_{D2}$	P_{D2}	P_{D1}	$Ch1_{D1}$
Cofactors, *a*	−13	7	1	−15	21	−57	−83	27	103	123	237	206
Mn_4Ca cluster	—	—	—	—	—	—	—	—	47	100	214	160
Side chains, *b*	−38	−19	35	47	−121	−84	−85	−123	48	−12	−135	−85
Backbone, *c*	22	93	59	23	71	40	43	62	150	192	223	80
Total, *a* + *b* + *c*	−29	81	95	55	−29	−101	−125	−34	301	303	325	201

E_m is relative to the solution values E_m(Chl*a*) = 800 mV (8, 9) and E_m(BChl*a*) = 640 mV (7) in CH_2Cl_2 in units of millivolts. —, not applicable.

dielectric continuum of $\varepsilon_p = 4$ is considered. In the D1/D2/CP43/CP47 core of PSII, the calculated $E_m(P_{D1/D2})$ is 1,096/1,093 mV, resulting in an up-shift of 64/74 mV relative to the D1/D2 core. These $E_m(P_{D1/D2})$ are still significantly higher than $E_m(P_{A/B})$ = 587/599 mV calculated for the native PSI complex [$E_m(P_{A/B})$ = 593/610 mV for the PsaA/PsaB core]. In the following two paragraphs, we focus on the D1/D2 core, the simplified PSII system.

Negligible discrimination from protein dielectric volume. The influence of the dielectric environment of the protein that might be possibly lower in PSII than PSI was speculated to be a major factor of the high E_m of P680 in PSII by Hasegawa and Noguchi (23). However, Rutherford and Faller (24) suggested that there is no reason to assume that the dielectric environment in PSII is different compared with the other RC. One of the remarkable findings of the present study is that the E_m(Chl*a*) values calculated by considering merely the protein dielectric volume (i.e., the space covered by the merged van der Waals volumes of protein atoms) and neglecting atomic charges do not differ greatly between PSII and PSI, in agreement with the latter suggestion (24) (Figs. 2 and 4). Thus, in contrast to the apparent structural difference (Fig. 1), the substantial influence of protein dielectric volume (i.e., protein shape) on E_m(Chl*a*) is essentially the same in both proteins.

E_m difference of 400–450 mV due to atomic charges. The majority of the 600-mV E_m difference between $P_{D1/D2}$ and $P_{A/B}$ originates from the protein atomic charges. They are responsible for a dramatic up-shift of 325/303 mV for $E_m(P_{D1/D2})$ in PSII, as opposed to a down-shift of 125/101 mV for $E_m(P_{A/B})$ in PSI. Hence, the atomic charge distribution of the proteins yield a net E_m difference of 400–450 mV between $P_{D1/D2}$ and $P_{A/B}$ (Table 1). In the following, we describe the details of atomic charge influences for bacterial RC, PSI, and PSII.

Mn_4Ca Cluster and Side Chains in the RC of PSII. In PSII, the direct influence of cofactors, especially of the Mn_4Ca cluster coordinated to D1, up-shift $E_m(P_{D1})$ and $E_m(Chl_{D1})$ by 214 and 160 mV, respectively (Table 1), whereas the up-shift of $E_m(P_{D2})$ and $E_m(Chl_{D2})$ is much smaller (100 and 47 mV, respectively). Charged side chains in PSII RC down-shift $E_m(P_{D1})$ by 135 mV but leave $E_m(P_{D2})$ essentially invariant (Table 1), thereby partially compensating influences from the Mn_4Ca cluster. Indeed, to energetically adjust the positively charged Mn_4Ca cluster on the D1 side in PSII, there are more acidic and less basic residues on the D1 side than on the D2 side. For a detailed discussion of side-chain influence, see supporting information. These data suggest that the combined influences of the Mn_4Ca cluster and side chains yield smaller E_m differences of ≈100 mV between P_{D1} and P_{D2} (Table 1).

Influences of the TMHs Harboring the Chlorophyll Pair in PSI and PSII. The up-shifts of E_m(Chl*a*) induced by protein backbone are significantly larger in the RC of PSII than of PSI (Table 1). The discussion below on PSII also holds true for PbRC. The strong influence of TMH $\mathbf{d}_{D1}$ in PSII, which up-shifts $E_m(P_{D1/D2})$ by 95 mV, is remarkable (supporting information). Notably, TMHs $\mathbf{d}_{D1/D2}$ provide the His-axial ligands to $P_{D1/D2}$ (D1-His-198/D2-His-197). However, the corresponding TMHs **j** in PSI (PsaA 670–691/PsaB 650–671) engender down-shifts of $E_m(P_A)$ and $E_m(P_B)$ by 28 and 27 mV, respectively (Fig. 3*a*).

The TMHs **d** in PSII and TMHs **j** in PSI are of similar length, but the histidines that coordinate the Chl*a* of $P_{D1/D2}$ and $P_{A/B}$ are located at different positions. In PSII, these histidines are at the luminal ends of TMHs **d**, as opposed to their more central positions in TMHs **j** of PSI (red translucent parts of TMHs **j** in Fig. 3*a*). In TMH **j** of PSI upstream of these His ligands, there are still eight more residues (PsaA 670–677/PsaB 650–657) (red translucent ribbons in Fig. 3*a*) relative to the situation in PSII. The protein backbone dipoles of these eight residues in TMH **j** of PSI stabilize the $P_{A/B}^{+\cdot}$ charge state dramatically. After removing these eight residues, the remaining parts of TMHs **j** in PSI (blue solid ribbons in Fig. 3*a*) have a direct influence that up-shifts $E_m(P_A)$ and $E_m(P_B)$ by 104 and 108 mV, respectively. Similar up-shifts of 95 mV were computed as a direct influence originating from the entire TMH $\mathbf{d}_{D1/D2}$ for $E_m(P_{D1})$ and $E_m(P_{D2})$ in PSII (Fig. 3*a*). Hence, the charges of the structurally different parts of the TMH $\mathbf{j}_A$ and $\mathbf{j}_B$ backbone in PSI (red translucent ribbons in Fig. 3*a*) down-shift $E_m(P_{A/B})$ by ≈130–140 mV relative to $E_m(P_{D1/D2})$ in PSII (red numbers in Fig. 3*a*).

Influence of Luminal α-Helices cd on $E_m(P_{D1/D2})$ in PSII Relative to $E_m(P_{L/M})$ in PbRC. The luminal α-helices cd and the segments connecting TMHs **c** and **d** in PSII (Fig. 3*c*) were proposed to play an important role in the energetics of $P680^{+\cdot}$ (25–27). The α-helix $\mathbf{cd}_{D1}$ of PSII (D1-176–190) is four residues longer than the α-helix $\mathbf{cd}_L$ of PbRC (L152–162) [i.e., D1-187–190 that up-shifts $E_m(P_{D1/D2})$ by 48/22 mV (Fig. 3*b*)]. There are other significant differences in this region between PbRC and PSII: (*i*) in PSII, D1-His-190/D2-His-189 (at or near the C termini of α-helices $\mathbf{cd}_{D1/D2}$) are H bond partners (D1-His-190 and D1-Glu-189) for the redox-active tyrosine Y_Z (D1-Tyr-161) located on TMH $\mathbf{c_{D1}}$ (Fig. 3*b*) and (*ii*) in PbRC, His-L153/His-M182 near the N termini of α-helices $\mathbf{cd}_{L/M}$ are axial ligands for BChl*a* of $BChl_{L/M}$ (Fig. 3*c*), whereas in PSII, the corresponding $Chl_{D1/D2}$ possess no axial ligands. These structural differences in this region give rise to a difference of 90–110 mV between $E_m(P_{D1/D2})$ and $E_m(P_{L/M})$ (supporting information).

Conclusion

E_m Difference of 600 mV Between $P_{D1/D2}$ in PSII and $P_{A/B}$ in PSI. The calculated $E_m(P_{D1/D2})$ for the complete PSII complex lies be-

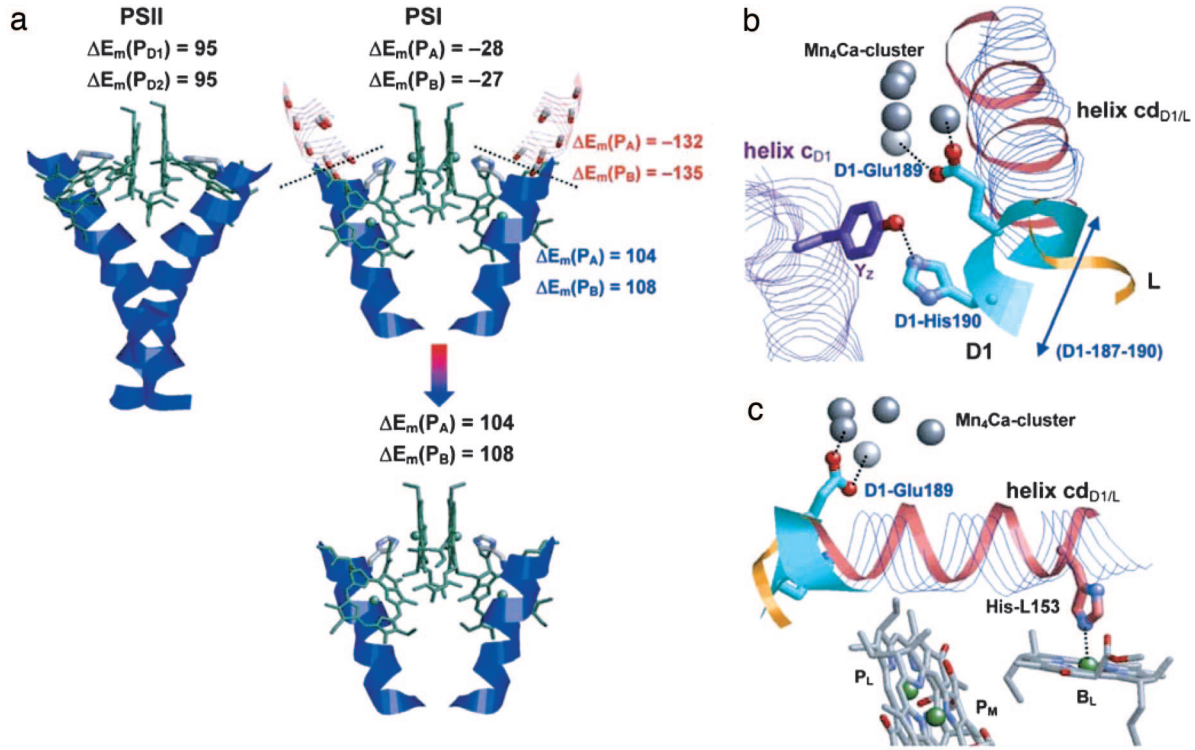

Fig. 3. Specific protein components influencing the Chl*a* pair redox potentials in PSI and PSII differently. (*a*) Different geometries of TMHs harboring His that axially coordinate $P_{A/B}$ in PSI (*Right*) or $P_{D1/D2}$ in PSII (*Left*). Black type indicates E_m shifts (ΔE_m) due to the direct influence of backbone charges from the whole TMHs **j** or **d** on $E_m(P_{A/B})$ or $E_m(P_{D1/D2})$, respectively. ΔE_m arising from the direct influence of backbone dipoles on removed and remaining parts of these TMHs are shown in red and blue type, respectively. (*b*) Arrangement of α-helix $\mathbf{cd}_{D1}$ on the D1 side in PSII relative to $\mathbf{cd}_L$ in PbRC. The α-helices **cd** and **c** in PSII are shown by blue translucent ribbons, and in PbRC, they are shown by pink solid ribbons. The green turn $\mathbf{cd}_{D1}$-187–190 in PSII has no corresponding helix region in bacterial RC. The redox-active tyrosine Y_Z hydrogen-bonds to D1-His-190 and D1-Glu-189, which coordinate the Mn_4Ca cluster. (*c*) Ligation of the accessory BCl*a* (B_L) in PbRC to His-L153 from α-helix $\mathbf{cd}_L$ (solid green, pink, and orange ribbons). The corresponding His is absent in α-helix $\mathbf{cd}_{D1}$ of PSII (blue translucent ribbon and green turn with D1-Glu-189).

tween 1,200 and 1,220 mV. Even for the D1/D2 RC alone, $E_m(P_{D1/D2})$ lies between 1,020 and 1,030 mV, which is still considerably high. Hence, the protein subunits peripheral to D1/D2 up-shift $E_m(P_{D1/D2})$ by 170–200 mV. This result contrasts with PSI, where the calculated $E_m(P_{A/B})$ in both the complete PSI complex and the RC formed by PsaA and PsaB lies between 590 and 600 mV. Elimination of the atomic charges in D1/D2 RC in PSII yields $E_m(P_{D1/D2})$ of 710–720 mV. Elimination of the atomic charges in the RC of PSI yields the same values for $E_m(P_{A/B})$ of 710 to 720 mV, indicating that the protein dielectric volumes of the RC in PSI and PSII do not give rise to a difference between $E_m(P_{A/B})$ and $E_m(P_{D1/D2})$.

The combination of charges of cofactors, side chains, and backbone in D1/D2 up-shifts $E_m(P_{D1/D2})$ by 300–330 mV, whereas the combination in the RC of PSI down-shifts $E_m(P_{A/B})$ by 100–130 mV (Table 1). As a consequence, the atomic charges in the protein environment give rise to a difference of 400–460 mV between $E_m(P_{A/B})$ and $E_m(P_{D1/D2})$. Specifically, the charges of the Mn_4Ca cluster up-shift $E_m(P_{D1/D2})$ by 210/100 mV.

Relative to $E_m(P_{D1/D2})$, the protein backbone dipoles down-shift $E_m(P_{A/B})$ by 150–180 mV. Most remarkable are the different geometries of the TMHs that harbor the His-ligands for $P_{D1/D2}$ (D1-His-198/D2-His-197) or $P_{A/B}$ (PsaA-His-680/PsaB-His-660). In TMH **j** of PSI, there are eight more residues (PsaA 670–677/PsaB 650–657) upstream of these His ligands relative to the situation in PSII. The protein backbone dipoles of these eight residues in TMH **j** of PSI stabilize the $P_{A/B}^{+\cdot}$ charge state dramatically, giving rise to a 130- to 140-mV down-shift in $E_m(P_{A/B})$ relative to $E_m(P_{D1/D2})$. In this regard, the TMH **d** in PSII and PbRC has the same influence on $E_m(P_{D1/D2})$ and $E_m(P_{L/M})$.

E_m Difference of 600 mV Between $P_{L/M}$ in PbRC and $P_{D1/D2}$ in PSII. The calculated $E_m(P_{L/M})$ lies between 640 and 660 mV. This finding is consistent with the 640 mV measured for the $E_m(P_L)$ of mutant His(M202)Leu of PbRC, which is generally assumed to yield the E_m for the uncoupled monomers of the BChl*a* pair (6). Thus, the measured E_m(P870) in PbRC is lower by 140–160 mV than the computed value because of the neglect of electronic coupling between P_L and P_M in the latter case.

The peripheral subunits of D1/D2 in PSII up-shift $E_m(P_{D1/D2})$ by 170–200 mV, whereas no corresponding shift was found for PbRC that does not possess these subunits.

Relative to $E_m(P_{L/M})$, the protein backbone dipoles up-shift $E_m(P_{D1/D2})$ by 100–160 mV. The major part of this difference (90–110 mV) originates from the luminal cytoplasmic segments D1-176–195/D2-176–194 in PSII and L152–170/M179–199 in PbRC. The remaining 160 mV of the 600-mV difference between PSII and PbRC is due to the intrinsically different E_m values of Chl*a* and BChl*a*.

Computational Procedures

Coordinates. We used the crystal structures for PSI at 2.5-Å resolution (Protein Data Bank ID code 1JB0) (13) and PSII at 3.0-Å resolution (PDB ID code 2AXT) (14) from the thermophilic cyanobacterium *Thermosynechococcus elongatus*. For WT PbRC, we used the crystal structures of PbRC from *R. sphaeroides* at 2.65-Å resolution (PDB ID code 1PCR) (10), at 2.2-Å resolution (PDB ID code 1AIJ, the dark-adapted structure), and at 2.6-Å

resolution (PDB ID code 1AIG, the light-exposed structure) (11). For the PbRC mutant His(M202)Leu, we used the crystal structure at 2.55-Å resolution (PDB ID code 1KBY) (12).

As described in previous applications (2, 28, 29), hydrogen atom positions were energetically optimized with CHARMM (30), keeping the positions of all nonhydrogen atoms fixed at crystallographically determined coordinates while all titratable groups were in their standard protonation states [i.e., acidic groups ionized and basic groups (including titratable histidines) protonated]. His residues that are ligands of Chl*a* were treated as nontitratable with neutral charge. The cytochromes b_{559} and c_{550} in PSII were kept in the reduced state; the other redox-active cofactors were in the neutral charge states.

Atomic Partial Charges. Atomic partial charges of the amino acids were adopted from the all-atom CHARMM22 (30) parameter set. For cofactors and residues whose charges are not available in CHARMM22, we used atomic partial charges from previous applications [PbRC (28), PSI (29), and PSII (2)].

For the Mn_4Ca cluster, we used essentially the same charge model as previously (see ref. 2), where the previous crystal structures at 3.2-Å resolution (PDB ID code 1W5C) (31) and 3.5-Å resolution (PDB ID code 1S5L) (32) were used. Although the structure at 3.0-Å resolution (14) features an additional Ca^{2+} ion as a component of the Mn_4Ca cluster as well as that at 3.5-Å resolution (32), the exact configuration of the Mn_4Ca cluster remains unclear. In the previous computation for the structures at 3.2-Å and 3.5-Å resolution, despite their different atomic models, we used the same net charge of the Mn_4Ca cluster for both structures. In the present study, although we assigned a charge of +2 to the newly determined Ca^{2+} ion, we used the same net charge of the Mn_4Ca cluster as in ref. 2. All computations were performed in the S1 resting state of the Mn_4Ca cluster with the corresponding charge distribution.

Computational Model for Chl*a*/BChl*a*. The Chl*a* of the dimer $P_{A/B}$ in PSI and of the pseudo-dimer $P_{D1/D2}$ in PSII are ligated by histidines, whereas the accessory Chl*a* ($A_{-1A/B}$) in PSI and $Chl_{D1/D2}$ in PSII are not. In case of the accessory Chl*a*, we used the same atomic charges as in the previous studies for PSI (29) and PSII (2). The atomic charges for the His-ligated Chl*a* for $P_{D1/D2}$ and $P_{A/B}$ and the His-ligated BChl*a* for $P_{L/M}$ and $BChl_{L/M}$ are listed in the supporting information.

E_m(Chl*a*) and E_m(BChl*a*) for one-electron oxidation have been experimentally measured in several solvents (reviewed in ref. 33). In the present study, we consider those measured in CH_2Cl_2 because only in CH_2Cl_2 are both E_m(Chl*a*) and E_m(BChl*a*) available. E_m(Chl*a*) was measured to be 800 mV (versus normal hydrogen electrode) in CH_2Cl_2 with tetrabutylammonium perchlorate as an electrolyte (8, 9). Taking into account the solvation energy difference between CH_2Cl_2 and water, we used the value of 698 mV as a reference E_m for Chl*a* in water (for details regarding the influence of electrolyte and water contamination, see supporting information). We evaluated the influence of a His ligand on E_m(Chl*a*) based on the calculated E_m(Chl*a*) of both model systems with and without His ligand and used the value of 585 mV as a reference E_m for His-ligated Chl*a* in water. For P_A in PSI, Chl*a* occurs as $C13^2$ epimer (Chl*a*′) (34), for which experimental E_m values are not available. Because of the increased steric energy between 13^2-methyl ester and 17-propionic ester, Chl*a*′′ is thermodynamically slightly less stable than Chl*a* (reviewed in ref. 35), which may result in a minor E_m shift of, at most, a few tens of millivolts. Therefore, we used the same E_m value as that used for conventional Chl*a*. This approximation will not significantly affect the difference in E_m(Chl*a*) of ≈600 mV between PSI and PSII. E_m(BChl*a*) for one-electron oxidation was measured to be 640 mV (versus normal hydrogen electrode) in CH_2Cl_2 (7). As with Chl*a*, we calculated the influence of the His ligand, yielding E_m(BChl*a*) = 427 mV as a reference E_m for His-ligated BChl*a* in water. For a discussion of E_m((B)Chl*a*) in different solvents, see ref. 33 and supporting information.

Computation of E_m(Chl*a*) and E_m(BChl*a*) in Proteins. The computation of the energetics of the protonation pattern of titratable residues and cofactors in proteins is based on the electrostatic continuum model, in which the linearized Poisson–Boltzmann (LPB) equation is solved by the program MEAD from Bashford and Karplus (36). To sample the ensemble of protonation patterns by a Monte Carlo (MC) method, we used our own program, KARLSBERG (37, 38). The dielectric constant was set to $\varepsilon_P = 4$ inside the protein and $\varepsilon_W = 80$ for solvent and possible protein cavities. For evaluation of the dielectric constant in the protein, see supporting information. Crystal water could not be observed in the PSII structure at 3.0-Å resolution. All computations were performed at 300 K, pH 7.0, and an ionic strength of 100 mM. The LPB equation was solved by a three-step grid-focusing procedure with a starting, intermediate, and final grid of 2.5-, 1.0-, and 0.3-Å resolution. MC sampling yields the probabilities $[A_{ox}]$ and $[A_{red}]$ of the oxidized and reduced states of the redox-active compound A, respectively. The E_m(Chl*a*) and E_m(BChl*a*) values in the protein environment were calculated from the Nernst equation. We varied the solvent potential such that we obtained an equal amount of both redox states ($[A_{ox}] = [A_{red}]$) at the $E_m(A)$. For convenience, the computed E_m values are given with millivolt accuracy, without implying that the last digit is significant. Systematic errors, which typically relate to specific conformations that may differ from the given crystal structures, can sometimes be considerably larger. Because the present study was performed under the same conditions as in previous computations, further details on error estimates and comparisons with the previous results can be obtained from refs. 2, 28, and 29.

We thank Dr. Dennis Diestler for improving the manuscript. This work was supported by Deutsche Forschungsgemeinschaft Sonderforschungsbereich 498 (Projects A4 and A5).

1. Rappaport, F., Guergova-Kuras, M., Nixon, P. J., Diner, B. A. & Lavergne, J. (2002) *Biochemistry* **41,** 8518–8527.
2. Ishikita, H., Loll, B., Biesiadka, J., Saenger, W. & Knapp, E.-W. (2005) *Biochemistry* **44,** 4118–4124.
3. Groot, M. L., Pawlowicz, N. P., van Wilderen, L. J. G. W., Breton, J., van Stokkum, I. H. M. & van Grondelle, R. (2005) *Proc. Natl. Acad. Sci. USA* **102,** 13087–13092.
4. Williams, J. C., Alden, R. G., Murchison, H. A., Peloquin, J. M., Woodbury, N. W. & Allen, J. P. (1992) *Biochemistry* **31,** 11029–11037.
5. Brettel, K. (1997) *Biochim. Biophys. Acta* **1318,** 322–373.
6. Allen, J. P., Artz, K., Lin, X., Williams, J. C., Ivancich, A., Albouy, D., Mattioli, T. A., Fetsch, A., Kuhn, M. & Lubitz, W. (1996) *Biochemistry* **35,** 6612–6619.
7. Fajer, J., Brune, D. C., Davis, M. S., Forman, A. & Spaulding, L. D. (1975) *Proc. Natl. Acad. Sci. USA* **72,** 4956–4960.
8. Fajer, J., Fujita, I., Davis, M. S., Forman, A., Hanson, L. K. & Smith, K. M. (1982) in *Electrochemical and Spectrochemical Studies of Biological Redox Components*, ed. Kadish, K. M. (Am. Chem. Soc., Washington, DC), Vol. 201, pp. 489–513.
9. Maggiora, L. L., Petke, J. D., Gopal, D., Iwamoto, R. T. & Maggiora, G. M. (1985) *Photochem. Photobiol.* **42,** 69–75.
10. Ermler, U., Fritzsch, G., Buchanan, S. K. & Michel, H. (1994) *Structure (London)* **2,** 925–936.
11. Stowell, M. H. B., McPhillips, T. M., Rees, D. C., Solitis, S. M., Abresch, E. & Feher, G. (1997) *Science* **276,** 812–816.
12. Camara-Artigas, A., Magee, C., Goetsch, A. & Allen, J. P. (2002) *Photosynth. Res.* **74,** 87–93.
13. Jordan, P., Fromme, P., Witt, H. T., Klukas, O., Saenger, W. & Krauss, N. (2001) *Nature* **411,** 909–917.

14. Loll, B., Kern, J., Saenger, W., Zouni, A. & Biesiadka, J. (2005) *Nature* **438,** 1040–1044.
15. Creighton, S., Hwang, J. K., Warshel, A., Parson, W. W. & Norris, J. (1988) *Biochemistry* **27,** 774–781.
16. Parson, W. W., Chu, Z.-T. & Warshel, A. (1990) *Biochim. Biophys. Acta* **1017,** 251–272.
17. Gunner, M. R., Nicholls, A. & Honig, B. (1996) *J. Phys. Chem.* **100,** 4277–4291.
18. Zhang, L. Y. & Friesner, R. A. (1998) *Proc. Natl. Acad. Sci. USA* **95,** 13603–13605.
19. Mattioli, T. A., Williams, J. C., Allen, J. P. & Robert, B. (1994) *Biochemistry* **33,** 1636–1643.
20. Johnson, E. T., Müh, F., Nabedryk, E., Williams, J. C., Allen, J. P., Lubitz, W., Breton, J. & Parson, W. W. (2002) *J. Phys. Chem. B* **106,** 11859–11869.
21. Reimers, J. R. & Hush, N. S. (2004) *J. Am. Chem. Soc.* **126,** 4132–4144.
22. Dekker, J. P. & van Grondelle, R. (2000) *Photosynth. Res.* **63,** 195–208.
23. Hasegawa, K. & Noguchi, T. (2005) *Biochemistry* **44,** 8865–8872.
24. Rutherford, A. W. & Faller, P. (2003) *Philos. Trans. R. Soc. London B* **358,** 245–253.
25. Manna, P., LoBrutto, R., Eijckelhoff, C., Dekker, J. P. & Vermaas, W. (1998) *Eur. J. Biochem.* **251,** 142–154.
26. Mulkidjanian, A. Y. (1999) *Biochim. Biophys. Acta* **1410,** 1–6.
27. Keilty, A. T., Vavilin, D. V. & Vermaas, W. F. J. (2001) *Biochemistry* **40,** 4131–4139.
28. Ishikita, H. & Knapp, E.-W. (2005) *Proc. Natl. Acad. Sci. USA* **102,** 16215–16220.
29. Ishikita, H. & Knapp, E.-W. (2003) *J. Biol. Chem.* **278,** 52002–52011.
30. Brooks, B. R., Bruccoleri, R. E., Olafson, B. D., States, D. J., Swaminathan, S. & Karplus, M. (1983) *J. Comput. Chem.* **4,** 187–217.
31. Biesiadka, J., Loll, B., Kern, J., Irrgang, K.-D. & Zouni, A. (2004) *Phys. Chem. Chem. Phys.* **6,** 4733–4736.
32. Ferreira, K. N., Iverson, T. M., Maghlaoui, K., Barber, J. & Iwata, S. (2004) *Science* **303,** 1831–1838.
33. Watanabe, T. & Kobayashi, M. (1991) in *Chlorophylls*, ed. Scheer, H. (CRC, Boca Raton, FL), pp. 287–303.
34. Watanabe, T., Kobayashi, M., Hongu, A., Nakazato, M., Hiyama, T. & Murata, N. (1985) *FEBS Lett.* **191,** 252–256.
35. Webber, A. N. & Lubitz, W. (2001) *Biochim. Biophys. Acta* **1507,** 61–79.
36. Bashford, D. & Karplus, M. (1990) *Biochemistry* **29,** 10219–10225.
37. Rabenstein, B. (1999) KARLSBERG, *A Monte Carlo pH and Redox Titration of Proteins Program* (Free University Berlin, Berlin).
38. Rabenstein, B. & Knapp, E.-W. (2001) *Biophys. J.* **80,** 1141–1150.